

Connections between the Long-Period Variability Modes of Both Temperature and Depth of the Upper Mixed Layer of the North Atlantic and the Climate Variability Indices

P. A. Sukhonos^{a, *} and N. A. Diansky^{b, c, d, **}

^a*Institute of Natural and Technical Systems, Sevastopol, 299011 Russia*

^b*Zubov State Oceanographic Institute, Moscow, 119034 Russia*

^c*Moscow State University, Moscow, 119991 Russia*

^d*Marchuk Institute of Numerical Mathematics, Russian Academy of Sciences, Moscow, 119333 Russia*

*e-mails: pasukhonis@mail.ru

**e-mails: nikolay.diansky@gmail.com

Received October 15, 2019; revised December 24, 2019; accepted February 5, 2020

Abstract—The interannual–multidecadal variability of the temperature and depth of the upper mixed layer (UML) in the North Atlantic (NA) is analyzed on the basis of the ORA-S3 ocean reanalysis data for 1959–2011. A large part of the UML in the NA is characterized by warming and thinning in all seasons in the period under study. After removing a linear trend, the UML temperature and depth anomalies in individual seasons are decomposed into empirical orthogonal functions (EOF). It is found that the three leading EOFs describe more than 50% of the total variability of the UML temperature and depth. The structure of the first EOF is horseshoe-shaped; this EOF represents coherent changes in the UML temperature and depth throughout the NA, which manifest themselves the year round. This mode corresponds to the Atlantic multidecadal oscillation. The spatial structure of the second EOF in the winter–spring period is a tripole and is caused by the North Atlantic Oscillation (NAO). The time coefficient of the second EOF of the UML temperature in the NA and the NAO index strongly correlate both synchronously and when the NAO index is 11 years ahead. The second EOF of the UML temperature in the summer–autumn period is associated with the Atlantic meridional mode. The third EOF is typical for the UML temperature fluctuations in January and corresponds to the East Atlantic Pattern.

Keywords: empirical orthogonal functions, upper mixed layer, temperature, interannual–multidecadal variability, the North Atlantic

DOI: 10.1134/S0001433820030111

INTRODUCTION

The results of the fundamental study by J. Bjerknes [1] show that the interannual variability of the sea surface temperature (SST) is caused by heat fluxes on the sea surface, which, in turn, are caused by changes in the atmospheric circulation, while decadal or longer SST fluctuations are associated with changes in ocean circulation. In particular, the interannual variability of the subtropical gyre can be a response to the long-term atmospheric forcing (changes associated with the intensity and position of the subtropical maximum). The structures of coherent low-frequency variability in the ocean–atmosphere system, which partly confirm the results by J. Bjerknes, were later obtained with the use of long-term data arrays [2–6]. The authors of recent work [7] note that the interdecadal variability in the North Atlantic (NA) is a direct response of the upper mixed layer (UML) of the ocean to the stochastic atmospheric forcing without the participation of the

thermohaline circulation of ocean waters. The discussion about the role of the ocean in the formation of interdecadal variability continues [8, 9]. Hence, it is quite difficult to identify modes of interannual and multidecadal variability of the NA UML parameters associated with the atmosphere–ocean interaction.

Let us consider main climate signals that can be determined for the NA water area.

The natural long-period SST fluctuation in the NA is called the Atlantic Multidecadal Oscillation (AMO) [2, 10]. This is one of the main climate signals in the World Ocean temperature field on interannual-to-multidecadal scales, and its origin is not associated with the El Niño–Southern Oscillation (ENSO) [11]. Many studies show the AMO effect on climate conditions in the Northern Hemisphere.

The main climate signal in the air pressure field over the Atlantic–European sector is North Atlantic Oscillation (NAO) (see, for example, [12] and the bib-

liography therein). The NAO has several definitions, but it is generally a meridional dipole structure in the air pressure field over the NA. The climate signal that is second in significance is the East Atlantic pattern (EA). The EA is a well-defined monopole in the air pressure field south of Iceland. The NAO and EA strongly affect the atmospheric circulation and long-term weather changes in Europe [13].

The Atlantic meridional mode (AMM) is clearly pronounced in the interannual–decadal variability of the hydrophysical parameters of the tropical Atlantic. It differs from the “zonal” mode of the ENSO type in its physical nature [14]. This mode manifests itself in the form of an anomalous meridional SST gradient through the central latitude of the Intertropical Convergence Zone (ICZ) [15]. The SST anomalies in the tropical Atlantic show significant consistency with NAO and with the variability of the sea level pressure over Iceland and the Azores separately on two sides of the ICZ [16]. Assuming that the NAO affects the meridional modes, the authors of [14] suggest that the AMM can act as an effective conductor for the effect of the extratropical atmosphere on the tropics. In addition, the AMM and AMO strongly correlate with hurricane activity in the NA on the decadal scale. The AMM also strongly correlates with hurricane activity in the NA on an interannual scale [17]. Thus, tropical and extratropical modes of climate variability are interrelated.

To identify the self-consistent spatiotemporal structures in the fields of hydrophysical parameters, decomposition into the empirical orthogonal functions (EOFs) can be used successfully [18]. The SST anomalies are decomposed into EOFs in many works for various time periods and different NA regions. However, different authors use different data processing techniques. First and foremost, this refers to the spatiotemporal averaging of the source data. This can be one of the reasons for the inconsistency of the results. At the same time, the main, most energetic, EOF modes show a strong tendency to have the simplest spatial structure inside a region analyzed. This property leads to a strong dependence of EOFs on the shape of the spatial boundaries of a region. In addition, the results of the EOF analysis depend on the length of the time series, since individual modes of upper ocean layer temperature variability can make different contributions to the total dispersion at different time periods and, therefore, are time dependent. Thus, EOFs should be extremely carefully interpreted as physical/dynamic modes of variability; this interpretation should always be accompanied by the physical analysis of their generation.

The EOF analysis was apparently first applied to the SST field in the NA in [19]. The low-frequency winter climate variability over the NA was analyzed in [2] on the basis of observations over 90 years. The main spatiotemporal regularities in the SST and sea-level pressure variability in the Atlantic Ocean for 1856–1991

are described in [20]. Note that interannual fluctuations in hydrophysical fields are shown in simultaneous variations in the annual averages and characteristics of seasonal variability. This means that the annual variability of parameters of hydrophysical fields changes from year to year, which is confirmed in [21] for large-scale SST anomalies in the NA. Therefore, we analyze the spatiotemporal structures of the interannual and multidecadal variability of the monthly average UML temperatures and depth in the NA separately for different seasons. The results are based on the analysis of EOFs calculated from the detrended data of ORA-S3 ocean reanalysis. We set the goal to find the correlations between the EOF of the UML temperature and depth and the above-described climate signals.

DATA AND PROCESSING TECHNIQUE

The data on the monthly average UML temperature and depth are taken from the ORA-S3 ocean reanalysis array for the period from January 1959 to December 2011 [22]. The spatial resolution of these data is 1° and, in the equatorial zone ($\pm 10^\circ$ latitude), $0.3^\circ \times 1^\circ$ in latitude and longitude, respectively. In addition, we use data on the net ocean surface heat fluxes and the wind stress over the NA water area taken from the ERA-40 atmospheric reanalysis array [23] for the period from January 1959 to June 2002 and operational ERA-40 model analysis for July 2002 to December 2011. These heat and momentum fluxes are used as boundary conditions in the ORA-S3 ocean reanalysis model. The NA water area selected for this study is bounded by the coordinates 0° – 70° N and 80° – 10° W, which coincides with the water area of the AMO definition.

The UML depth is calculated from the selected reanalysis based on the semiempirical theory of turbulence [24]. According to this theory, the UML depth corresponds to the depth where the Richardson number attains a critical value of 0.3.

The average temperature is calculated for each month from 1959 to 2011 within the UML depth variable in space and time based on 3D data of the reanalysis selected. Then, the values of the temperature and UML depth are distinguished for individual months. Further, linear trends are removed from the UML temperature and depth time series at each node of the spatial grid. Linear trend parameters are calculated by the least-squares method. After this, the resulting arrays of UML temperature anomalies and depths are EOF decomposed separately for each calendar month over the period under study [25].

The monthly average AMO and AMM indices for 1948–2017 were taken from the website <https://www.esrl.noaa.gov/psd/data/climateindices/list/>. The monthly average NAO and EA for 1950–2017 were taken from <http://www.cpc.ncep.noaa.gov/data/teledoc/telecontents.shtml>.

Along with EOF decomposition, we use composite analysis, which consists of the following. The NAO, AMM, and EA indices, which exceed in absolute value one standard deviation, allowed us to identify anomalous years. These years are grouped into two samples which correspond to the positive and negative phases of each climate signal. Each phase for each index includes at least 7 abnormal years, which is no less than 15% of the length of the corresponding time series. For these groups of years, the average values, variances, and standard deviations of the UML temperature and depth are calculated at each node of the regular grid. Then, a “clean” climate signal in the NA UML temperature and depth is found for calendar months. For this, the difference between the sample averages at each grid node (the so-called difference composite) is determined. The statistical significance of the differences between composite anomalies in the periods under study is assessed by the standard algorithm with the use of Student’s *t*-test. We also use correlation analysis.

RESULTS

Analysis of Linear Trends in UML Temperature and Depth

According to the data used, most of the NA is characterized by a positive linear trend in the UML temperature. The highest coefficients of the linear trend are observed in the region of the Gulf Stream transition into the North Atlantic Current. Their values are 0.05, 0.08, 0.04, and 0.04°C/year in January, April, July, and October, respectively. The coefficients of the linear trend in the cold season noticeably exceed those in the warm season, which corresponds to stronger warming in the winter period. Inside the subpolar gyre, the coefficients of the linear trend in the UML temperature are negative, except for October. The contribution of the linear trend variance into the total variance of the UML temperature exceeds 30% in the latitudinal band 0°–10° N to the east of 40° W (except for April), in the region of Gulf Stream transition into the North Atlantic Current (except for July) and in the vicinity of the East Greenland Current in July. The contribution of the linear trend variance into the total variance of the UML temperature throughout the NA water area is 13.8, 9.4, 15.4, and 20.7% in January, April, July, and October, respectively.

In tropical and subtropical latitudes, there are regions where the UML depth is characterized by an insignificant positive linear trend in the winter months in 1959–2011. In high latitudes, significant negative linear trends in the UML depth were revealed for the period under study. The coefficient of the linear trend in the UML depth is 30 m/year in the region of intense convection in the Labrador Sea in January, which results in an almost twofold decrease in the average UML depth (from 3 to 1.5 km). After removing the

linear trend, the standard deviation of the UML depth is equal to ~1 km in this region in January. The UML depths, their standard deviations, and the coefficients of the linear trend in the summer months are smaller than in the winter months. Thus, processes which occur in high latitudes make the main contribution to the low-frequency variability of the NA UML depth. A decrease in this parameter is generally noted and is most pronounced in the cold season.

Thus, the NA UML is characterized by warming and thinning during the period under study. The latter occurs mainly due to the weakening of convective mixing in high latitudes. This might well be due to an increase in the Arctic Ocean temperature, the intensification of melting of Greenland glaciers, and the flowing of desalinated waters out of the Arctic Ocean in the second half of the 20th century [26]. Possible climate changes in the Northern Hemisphere if the oceanic heat influx in the NA ceases were estimated in [27]. Then, after detrending the time series, we analyze the interannual and multidecadal variability of the UML temperature and depth based on the EOF decomposition.

Main EOFs of the UML Temperature and Depth in the NA

The spatial structures of the first EOF of the NA UML temperature for each month are consistent with each other and are of horseshoe shape. The values have the same sign in most of the water area, while the region of the opposite sign is in the western part of the subtropical gyre (Fig. 1a). However, there are some differences between the structures in different months. The size of the region of the opposite sign in the western part of the subtropical gyre is maximal in April and minimal in October. The contribution of the first EOF to the total variability of the UML temperature in the NA is 29.6, 40.4, 18.3, and 21.8% in January, April, July, and October, respectively. The high contribution in April is explained by a change from winter mixed to summer stratified state, when high temperature anomalies spontaneously occur in UML at its small depth. The time coefficients of the first EOF of the NA UML temperature show the same variability on the interdecadal–multidecadal scale for each month of the year (Fig. 1c). This is manifested in a strong correlation between these time series. As for the multidecadal variability, there are long periods of low (e.g., in the early 1970s to the early 1990s) and high UML temperatures (e.g., in the late 1990s and 2000s). The correlation coefficients between the time coefficients of the first EOF of the NA UML temperature and the AMO index are 0.82 in January, 0.88 in April, 0.85 in July, and 0.88 in October in 1959–2011.

The spatial structures of the first EOF of the UML depth in the NA for each month are consistent with each other. The highest values of the same sign

are concentrated in the inner part of the subpolar gyre (Fig. 1b). The area of this region is maximal in the autumn–winter months and minimal in summer. The contribution of the first EOF to the total variability of the UML depth in the NA is 51.5, 40, 32.5, and 59.7% in January, April, July, and October, respectively. The correlation coefficient between the time coefficients of the first EOF of the UML depth is equal to 0.73 in January and April. A low-frequency quasi-sixty-year oscillation is manifested in the time coefficients of the first EOF of the UML depth in the NA for each month of the year, which is similar to the behavior of the AMO index. The correlation coefficient between the time coefficient of the first EOF of the UML depth and the AMO index is 0.69 in January in the period under study (Fig. 1c). The correlation coefficient between the time coefficient of the first EOF of the UML temperature and the time coefficient of the first EOF of the UML depth is 0.75 in January.

Thus, despite some local differences between months, the first EOFs of the UML temperature and depth in the NA correlate well with the AMO. This points out to the large-scale nature of this climate signal. The UML temperature increases with a decrease in the UML depth in the subpolar gyre during the positive AMO phase. Note that the amplitude of this EOF in the subpolar gyre can be underestimated because of averaging of the ocean temperature over deep UML, the depth of which can exceed 2000 m in January. This becomes possible in the upper ocean layer when regions of local heating are formed in it due to the winter interaction of the active ocean layer with the atmosphere [28].

The spatial structures of the second and third EOFs of the UML depth in the NA are regions of different signs within the subpolar gyre. The contributions of the second and third EOFs to the total variability of the UML depth are low; they are 8.7, 8, 10.3, and 8.6% for the second EOF and 5.8, 6, 9, and 5.6% for the third EOF in January, April, July, and October, respectively. We will not dwell on these EOFs of the UML depth in detail below; only note that, according to the data used, the variance of the UML depth throughout the NA water area is 19134, 17442, 2333, and 4631 m² in January, April, July, and October, respectively. This variance is approximately 7–8 times higher in the winter months than in the summer months. Therefore, despite the higher relative contribution (in %) of the second and third EOFs to the total variability of the UML depth in the summer months as compared to the winter months, the parts of the variance described by these EOFs are small in the summer months.

Let us analyze the second EOF of the NA UML temperature. Figure 2a shows its spatial structure for January and April. The structure of the second EOF in these months shows changes in the UML temperature of different signs in different latitudinal zones of

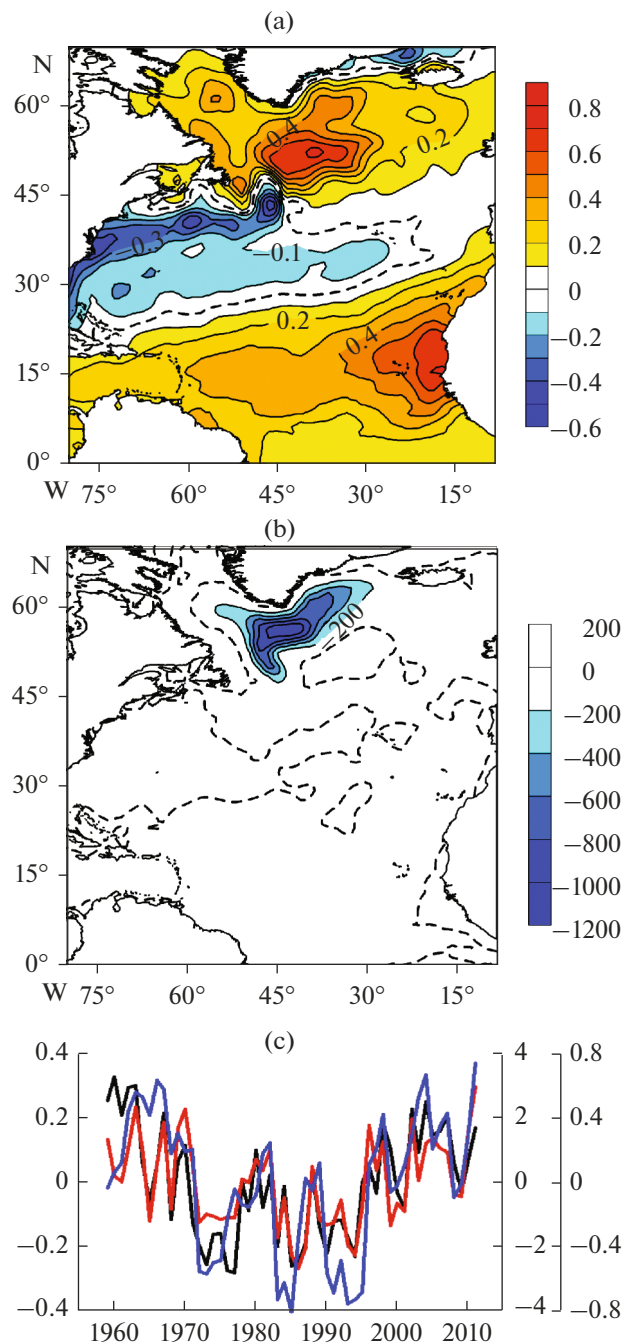


Fig. 1. Spatial structures of the first EOF of the (a) UML temperature and (b) depth in January; (c) corresponding time coefficients of the decomposition of the UML temperature (red curve, second scale on the right) and depth (blue curve, first scale on the right) and AMO index in January (black curve, left scale). The dashed curves in (a, b) show the zero isolines.

the NA. The changes in the spatial structure of this mode for January and April are insignificant and are mainly shown in an increase in the regions of the opposite signs in the western parts of the subtropical and subpolar gyres in April. This EOF describes from 11.3 (January) to 8.6% (April) of the total variability of

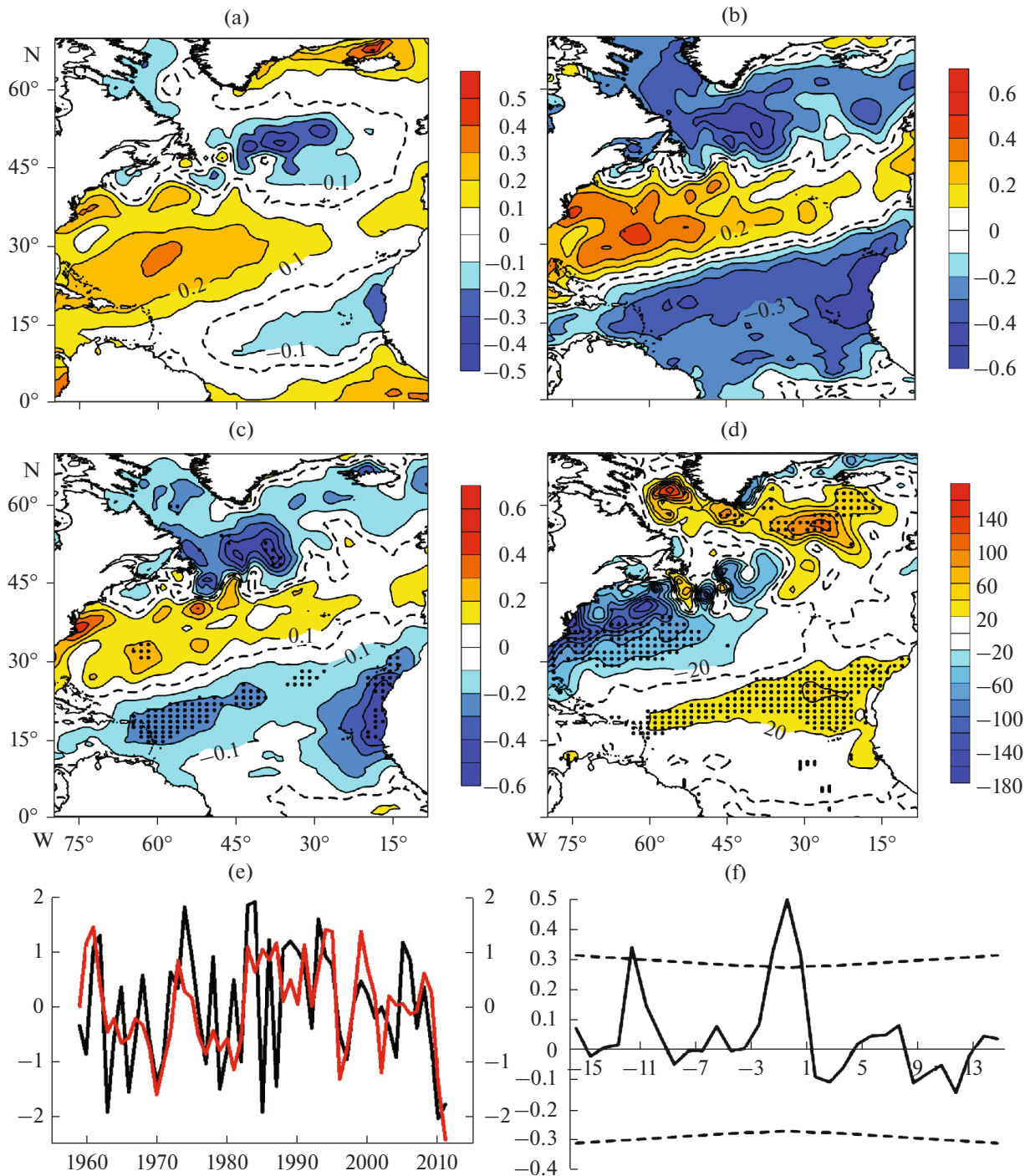


Fig. 2. (a) Spatial structure of the second EOF of the UML temperature in January; (b) spatial distribution of the correlation coefficients between the UML temperature and the NAO index in January; differences between (c) the UML temperature ($^{\circ}\text{C}$) and (d) net ocean surface heat fluxes (W/m^2 ; positive values correspond to the heat loss) anomalies during the positive and negative NAO phases in January; (e) time coefficients of the second EOF of the UML temperature (red curve, right scale) and the NAO index (black curve, left scale) in January; and (f) cross-correlation function between the time series shown in (e). Negative shifts (years) correspond to the advance in the NAO index. Dashed curves in (a–d) show the zero isolines. Black dots in (c, d) show the grid nodes, where the difference is statistically significant at a level of 90%. The dashed curves in (f) show the 95% confidence interval.

UML temperature in the NA. The correlation coefficient between them is 0.48 in January and April for 1959–2011. The time coefficients of the second EOF of the UML temperature show strong interannual

variability (Fig. 2e). The correlation coefficient between the time coefficient of the second EOF of the UML temperature and the NAO index is 0.51 after removing the linear trend in January.

The correlation analysis of the NAO index and the NA UML temperature at each grid node in January shows a close relationship between these characteristics, negative in the inner part of the subpolar gyre and in the West African upwelling region and positive in the inner part of the subtropical gyre (Fig. 2b).

The period under study includes 10 years with the positive phase (1974, 1983, 1984, 1986, 1989, 1990, 1993, 1994, 2005, and 2006) and 9 years with the negative phase of the NAO (1960, 1966, 1970, 1971, 1977, 1979, 1985, 1987, and 2010). The UML temperature during the positive NAO phase, as compared to the negative phase, is characterized by a statistically significant decrease by 0.4°C in the inner part of the subpolar gyre and in the West African upwelling region and an increase in the inner part of the subtropical gyre (Fig. 2c).

The spatial structures of the second EOF of the UML temperature (Fig. 2a), the field of the correlation coefficients between the UML temperature and the NAO index (Fig. 2b), and the difference composite (Fig. 2c) are very similar. A similar structure is also confirmed by the composite analysis of the net ocean surface heat fluxes during the positive and negative NAO phases (Fig. 2d). Regions with high heat loss from the ocean surface are located in the inner part of the subpolar gyre ($+70\text{ W/m}^2$) and in the Northern Equatorial Current ($+35\text{ W/m}^2$). A decrease in the heat release to the atmosphere is noted in the western part of the subtropical gyre (-45 W/m^2). Thus, the composite and correlation analysis confirm that the intensification of NAO is accompanied by a drop in the UML temperature in the regions of trade and westerly winds and its increase in subtropical latitudes. However, the signs of the heat flux and UML temperature anomalies are inconsistent to the east of Newfoundland along 45° N , where the extreme point of the northern cell of the EOF is located. This can be explained by a significant role of advection factors of formation of UML temperature anomalies here, since this region is influenced by the Gulf Stream and the North Atlantic Current.

The analysis of the cross-correlation function between the time coefficient of the second EOF of the UML temperature and the NAO index after detrending in January showed that the highest correlation coefficients of about 0.5 are observed at a zero shift between these time series (Fig. 2f). In addition, these time series strongly correlate when the NAO index is 11 years ahead.

The spatial structures of the second EOF of the UML temperature in the NA in July and October are similar. Figure 3a shows the spatial structure of the second EOF based on July data. The structure of this EOF is horseshoe-shaped, oriented from west to east, with values of one sign in the eastern part of the equatorial Atlantic, latitudinal band 35° – 50° N , and the East Greenland Current and values of the opposite sign

in the rest of the water area. The second EOF describes from 12 (July) to 10.5% (October) of the total variability of the UML temperature in the NA. The coefficient of correlation between the time coefficient of this EOF and the AMM index after detrending is equal to 0.47 for 1959–2011 (Fig. 3e). The AMM index in July shows pronounced 10-year variability: it decreases by the early 1970s and then increases.

The detrended AMM index and the UML temperature strongly correlate at each grid node in the NA, especially to the south of 25° N , in July (Fig. 3b); the correlation coefficients exceed 0.6 here. Thus, more than 35% of the total variability of the UML temperature in the tropical Atlantic in summer is due to the effect of the AMM.

The period under study includes 7 years with the positive AMM phase (1962, 1988, 1989, 1995, 2004, 2005, and 2010) and 9 years with the negative AMM phase (1972, 1973, 1974, 1984, 1986, 1991, 1993, 1994, and 2002). During the positive AMM phase, as compared to the negative phase, the UML temperature is characterized by a statistically significant increase in the inner part of the subpolar gyre, the eastern part of the subtropical gyre, and tropical latitudes (except for the eastern part of the equatorial Atlantic) (Fig. 3c). Negative UML temperatures are observed in the East Greenland Current. The analysis of the difference composite of the wind-stress module during the positive and negative AMM phases shows a significant decrease in this parameter during the positive AMM phase in the trade-wind region (-0.012 N/m^2) (Fig. 3d). Thus, it is confirmed that the intensification of the AMM in July is accompanied by UML warming in the tropical Atlantic and a decrease in the wind-stress modulus in the trade wind region.

Let us now consider the third EOF of the NA UML temperature. Figure 4a shows the spatial structure of this mode for January. One can see changes in the UML temperature of different signs: one sign in the vicinity of ICZ and to the north of 30° N , and the opposite sign in the latitudinal band 15° – 30° N . This EOF describes 8.2% (January) of the total variability of the NA UML temperature; its time coefficient is characterized by pronounced interdecadal variability. The correlation coefficient between this coefficient and the EA index after removing the linear trend is equal to 0.31 in January for 1959–2011 (Fig. 4b). The correlation between these time series after the removal of the parabolic trend is 0.33.

The period under study includes 10 years with the positive EA phase (1970, 1971, 1973, 1988, 1991, 2001, 2002, 2003, 2007, and 2009) and 8 years with the negative one (1963, 1965, 1968, 1969, 1976, 1981, 2000, and 2005). A statistically significant decrease of 0.3°C in the UML temperature during the positive EA phase, as compared to the negative phase, is observed within the region 35° – 45° N and 35° – 20° W . Positive UML temperatures are observed to the north of South

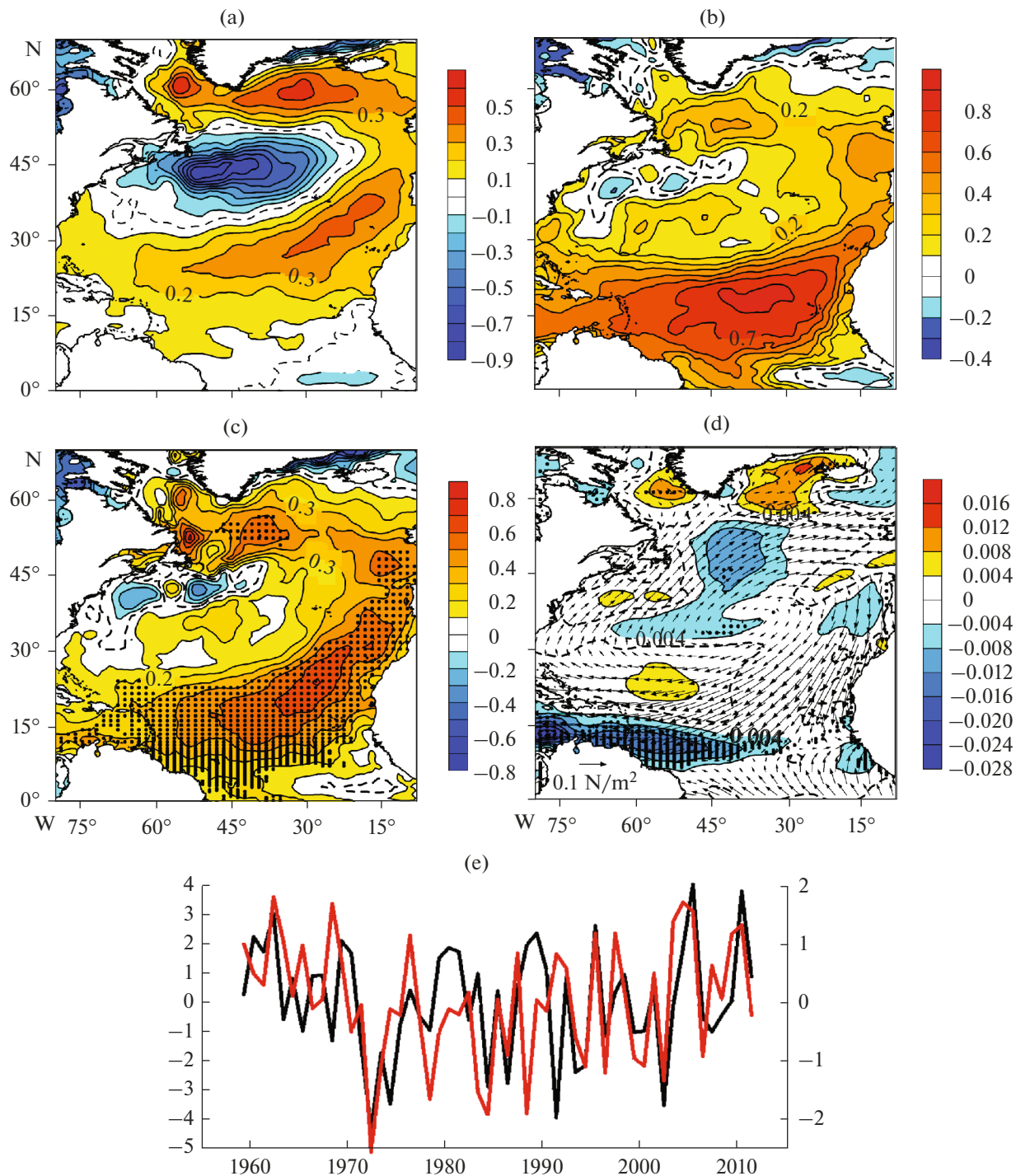


Fig. 3. (a) Spatial structure of the second EOF of the UML temperature in July; (b) spatial distribution of correlation coefficients between the UML temperature and the AMM index in July; differences between (c) the UML temperature ($^{\circ}\text{C}$) and (d) the wind-stress-modulus (N/m^2) anomalies during the positive and negative AMM phases in July; and (e) time coefficient of the second EOF of the UML temperature (red curve, right scale) and the AMM index (black curve, left scale). Dashed curves in (a–d) show the zero isolines. Black dots in (c, d) show the grid nodes, where the difference is statistically significant at a level of 90%. The vectors in (d) show the 1959–2011 averaged wind stress in July.

America ($+0.2^{\circ}\text{C}$) (Fig. 4c). Thus, the intensification of EA is accompanied by the cooling of UML in the vicinity of the Azores and warming in the Greater Antilles. This result is confirmed by the correlation

coefficients between the time series of the UML temperature and the EA index after the removal of the linear trend at each grid node in January (Fig. 4d). Note, however, that the third EOF describes a much

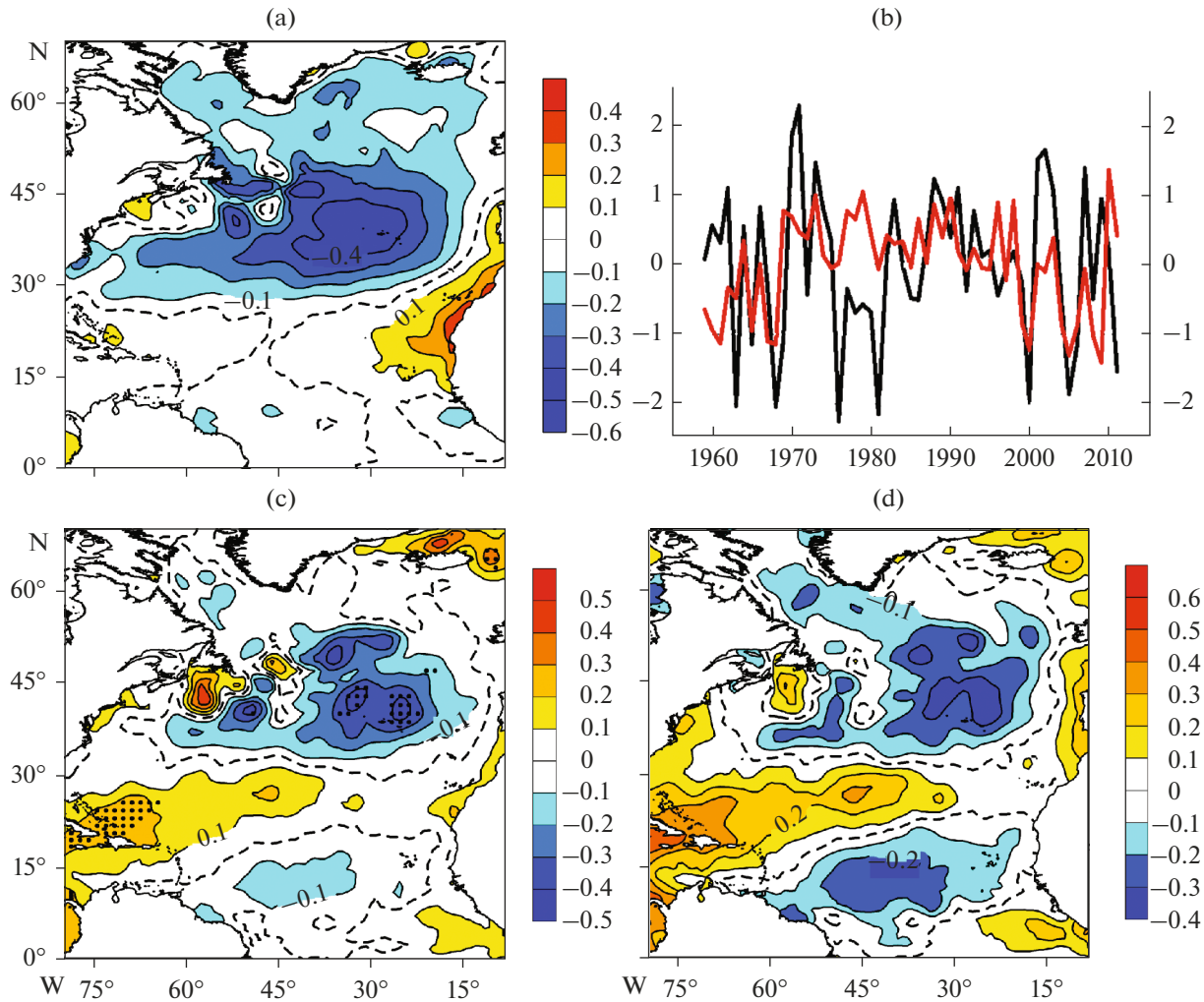


Fig. 4. (a) Spatial structure of the third EOF of the UML temperature in January; (b) time coefficient of the third EOF of the UML temperature (red curve, right scale) and the EA index (black curve, left scale) in January; (c) difference between the UML temperature anomalies ($^{\circ}\text{C}$) during the positive and negative EA phases in January; and (d) spatial distribution of the correlation coefficients between the UML temperature and the EA index in January. Dashed curves in (a, c, d) show the zero isolines. Black dots in (c) show the grid nodes, where the difference is statistically significant at a level of 90%.

smaller fraction of the total winter variability of the UML temperature.

The spatial structures of the third EOF of the UML temperature in April, July, and October are regions with different signs within the NA. The contribution of this EOF to the total variability of the UML temperature is low: 6, 10, and 7.7% in April, July, and October, respectively. The variance of UML temperature is 0.38, 0.28, 0.22, and 0.26°C^2 in January, April, July, and October, respectively, for the entire NA water area. This parameter is approximately 1.5 times higher in the winter months than in the summer months. Therefore, despite the large relative contribution (in %) of the third EOF to the total variability of the UML temperature from the summer months as compared to the winter months, the part of the variance described by this EOF in January is almost 1.5 times larger than the corresponding part of the dispersion of this EOF in July.

DISCUSSION

The variability of the NA UML depth was previously analyzed for 1960–2004 in [29]. The authors showed that the UML depth increased by 10–40 m in the central part of the NA during the winter–spring period for those 45 years. In that work, the UML depth was calculated using the temperature criterion. According to this criterion, the UML depth is defined as the depth at which the temperature changes by 0.2°C with respect to its value at a depth of 10 m. We emphasize that the difference and gradient criteria for UML depth estimation require the careful selection of the threshold values, since the resulting UML depth (and its long-period variability) strongly depend on the methodology for its estimation. High values of the temperature criterion apparently cover deeper gradients in the thermocline instead of the lower UML boundary, which is especially important under condi-

tions of low-temperature stratification in the northern NA (see, for example, Figs. 2g and 2i in [30]). It should be noted that the temperature difference criterion for UML depth estimation does not take into account the salinity contribution to the density. Therefore, it is more correct to use the density difference criterion. Note that the technique for determining the depth of the UML lower boundary by the Richardson number is more justified from the physical point of view. According to our data, the UML depth actually increased in the subtropics in the winter–spring period from 1960 to 2004. However, since the early 2000s, during the positive AMO phase, the intensity of the subtropical convective cell has weakened [31] and the UML depth in January has decreased on a multidecadal scale [32]. That resulted in a decrease in the long-term (1959–2011) winter deepening of the UML in the subtropics. As for the interannual–multidecadal variability of the UML depth for the entire NA (after removing the linear trend), the role of ocean processes at high latitudes is of great importance. Note that linear trends are separately analyzed and removed in this work, after which the UML parameters are analyzed. This is due to the fact that tendencies in the anthropogenic forcing and natural variability coincided in the UML in 1960–2004.

The maximal UML depth in the central part of the Labrador Sea was assessed in [33] on the basis of available observational data for 1993–2014. The winter maxima of the UML depth significantly decreased from the mid-1990s to the mid-2000s against the background of intense interannual variability. This fact is consistent with our assessments of the UML depth by the Richardson criterion.

According to our results, the AMO index can also be defined as the time coefficient of the first mode of EOF decomposition of the monthly average UML temperature or depth. This statement is probably true for the EOF decomposition of long time series (longer than or equal to the AMO period). For example, the Pacific Decadal Oscillation index is defined as the time coefficient of the first mode of monthly average SST decomposition in the North Pacific Ocean (to the north of 20° N) [34]. Our results also show the subpolar gyre to be a key region for the AMO formation and the importance of processes at the lower UML boundary in the evolution of variability on this scale. This conclusion does not agree with the results [7], obtained with the use of an extremely simplified model of the ocean with the constant-depth UML. This is an indirect confirmation of the important role of thermohaline circulation in the AMO formation defended in [8]. In addition, the Arctic ocean processes play a large role in maintaining the AMO [35, 36].

The spatial structure of the second EOF of the UML temperature, consistent with the NAO index, is tripole, where correlations with SST are positive in the Sargasso Sea and negative in the northwestern part of the tropical Atlantic and the vicinity of the Labrador

Sea (see, e.g., [4, 5, 37, 38] and others). This structure in the ocean–atmosphere system is associated with wind heat advection over the ocean [39]. As is shown in [4, 5], this mode in winter UML temperature anomalies is generated under the atmospheric forcing, which confirms the forced nature of this mode. The maximal correlation coefficient between the time coefficient of the second EOF of the UML temperature and the NAO index after detrending increases to approximately 0.75 when the atmospheric forcing is 0.5 months ahead [5], which is explained with the help of a simple analytical model for the evolution of UML temperature anomalies. The half-month shift of the delay of large-scale UML temperature anomalies in the midlatitudes is defined as a quarter of the period from the most significant period of fluctuations in the atmospheric forcing, which is about 2 months in the most energy-carrying range of NAO variability, since the low-frequency variability of the atmosphere in the monthly average fields is clearly manifested just in this period.

The increase in the correlation observed when the NAO index is 11 years ahead (Fig. 2f) cannot be explained by these simple considerations, since a minimum is observed in the NAO index spectrum in 10- to 40-year periods (see, for example, [40]). Therefore, the relationship between the UML temperature anomalies and the NAO 11 years ahead requires an explanation. Note that the typical time for the subtropical gyre to adapt to changing atmospheric forcing is about 10 years [41].

The authors of [42] suggested a correlation between the monopole mode south of Iceland (the third EOF of the UML temperature in January in the present work) and the ocean effect on atmospheric processes based on relatively short time series (1950–1987). Our results are based on long-term data; they show the coincidence of the third EOF of the UML temperature in January with the EA. Moreover, the EA significantly affects the UML temperature in several small NA regions. However, its contribution to the total winter variability of the UML temperature is the smallest in comparison with other modes under study.

Atmospheric circulation factors play an important role in the formation of the NA UML temperature variability in winter. In summer, winds and currents are weak in the NA and the UML depth is reduced. Hence, the atmospheric circulation indices, such as NAO and EA, correlate weakly with the time coefficients of the EOF decomposition of the UML temperature for the summer months. The summer NAO is characterized by lower amplitude when compared with the winter period and the northeastward displacement of its centers of action beyond the NA boundaries [43]. Therefore, in summer, this climate signal can no longer describe a large fraction of the variance of the NA UML parameters, and the role of tropical variability modes increases.

Changes in the intensity of the trade winds in the tropical Atlantic precede SST anomalies (and, therefore, the anomalous SST gradient at the central latitude of the ICZ): weaker (stronger) trade winds are accompanied by warmer (colder) SST anomalies [15]. In addition, this means that the “meridional” mode of the NA UML temperature variability is generated under an external forcing. The NAO can act as one of the sources of this forcing. However, another explanation of the meridional mode is a positive feedback between the wind speed, evaporation, and SST anomalies [44, 45] (although an external forcing is also required to maintain the meridional mode in this case).

The close relationship between the EOF decomposition modes of the UML temperature and individual processes in the ocean–atmosphere system is of interest. Since EOFs are mutually orthogonal by definition, there must also be a quasi-orthogonal AMO, NAO, EA, and AMM associated with them. This is partially confirmed by the small values of the synchronous correlation coefficients between the indices of the climate signals under study in different seasons.

CONCLUSIONS

We have analyzed the linear trends and interannual–multidecadal variability of the NA UML temperature and depth in different seasons. The results are based on the EOF decomposition of ORA-S3 ocean reanalysis data for 1959–2011.

Warming of the NA UML is noted, along with a decrease in its depth in the period under study. A positive linear trend in the UML temperature is pronounced in all months of the year in most of the NA water area, although negative trends are observed in some regions. Significant linear trends in the UML depth are mainly concentrated at high latitudes and better pronounced in the winter months. In summer, linear trends in the UML depth variability are also observed, but their coefficients are small.

The analysis of the main modes of NA UML temperature and depth after detrending shows the following. The three leading EOFs describe more than 50% of the total variability of the UML temperature and depth. The first EOF shows a coherent multidecadal variability of these parameters throughout the NA water area. Despite some differences in its spatial structure in individual months, this EOF is a manifestation of the AMO. The second EOF is characterized by a spatial structure with opposite signs in different latitudinal zones of the NA for UML temperature fluctuations in January and April. The contribution of this EOF to the total variability of the UML temperature is about half the contribution of the first EOF. This EOF is caused by the NAO. A significant correlation was found between the time coefficient of the second EOF of the UML temperature and the NAO index without the linear trend, both synchronously

and when the NAO is 11 years ahead. The second EOF for UML temperature variations in July and October is characterized by a spatial structure, where changes in the UML temperature have one sign in the eastern part of the equatorial Atlantic, North Atlantic, and East Greenland currents and the opposite sign in the rest of the NA water area. This EOF was found to correspond to the AMM. The third EOF of the UML temperature fluctuations coincides with the EA in January. However, its contribution to the total UML temperature variability is low.

Thus, only the lowest frequency mode shows the evolution of the AMO index, which can be associated with fluctuations in the thermohaline circulation in the NA. The second and third EOF modes are the response of the UML to the atmospheric forcing determined by the NAO, AMM, and EA. Moreover, the second UML temperature mode differs in nature in the cold and warm season.

ACKNOWLEDGMENTS

We are grateful to an anonymous reviewer for friendly and constructive criticism of the first version of the work and to the editorial board for their professional and prompt review of it.

FUNDING

This work (the analysis of interannual–multidecadal variability of the UML temperature and depth) was supported by the Russian Science Foundation, project no 17-17-01295 and (the EOF decomposition of the UML temperature and depth) by the Russian Foundation for Basic Research, project no. 18-05-01107.

REFERENCES

1. J. Bjerknes, *Atlantic Air–Sea Interaction*, vol. 10 of *Advances in Geophysics* (Academic Press, New York, 1964). [https://doi.org/10.1016/S0065-2687\(08\)60005-9](https://doi.org/10.1016/S0065-2687(08)60005-9)
2. C. Deser and M. L. Blackmon, “Surface climate variations over the North Atlantic Ocean during winter: 1900–1989,” *J. Clim.* **6** (9), 1743–1753 (1993).
3. Y. Kushnir, “Interdecadal variations in North Atlantic sea surface temperature and associated atmospheric conditions,” *J. Clim.* **7** (1), 141–157 (1994).
4. C. Deser and M. S. Timlin, “Atmosphere–ocean interaction on weekly timescales in the North Atlantic and Pacific,” *J. Clim.* **10** (3), 393–408 (1997).
5. N. A. Dianskii, “Temporal relationships and special forms of the combined modes of altitude anomaly for the 500 mb isobaric surface and ocean surface temperature in the North Atlantic Ocean in winter,” *Izv., Atmos. Ocean. Phys.* **34** (2), 197–213 (1998).
6. S. K. Gulev, M. Latif, N. Keenlyside, et al., “North Atlantic Ocean control on surface heat flux on multidecadal timescales,” *Nature* **499** (7459), 464–467 (2013). <https://doi.org/10.1038/nature12268>

7. A. Clement, K. Bellomo, L. N. Murphy, et al., “The Atlantic Multidecadal Oscillation without a role for ocean circulation,” *Science* **350** (6258), 320–324 (2015). <https://doi.org/10.1126/science.aab3980>
8. R. Zhang, R. Sutton, G. Danabasoglu, et al., “Comment on “The Atlantic Multidecadal Oscillation without a role for ocean circulation”,” *Science* **352** (6293), 1527 (2016). <https://doi.org/10.1126/science.aaf1660>
9. K. Bellomo, L. N. Murphy, M. A. Cane, et al., “Historical forcings as main drivers of the Atlantic multidecadal variability in the CESM large ensemble,” *Clim. Dyn.* **50** (9–10), 3687–3698 (2018). <https://doi.org/10.1007/s00382-017-3834-3>
10. M. E. Schlesinger and N. Ramankutty, “An oscillation in the global climate system of period 65–70 years,” *Nature* **367** (6465), 723–726 (1994). <https://doi.org/10.1038/367723a0>
11. D. B. Enfield and A. M. Mestas-Nunez, “Multiscale variabilities in global sea surface temperatures and their relationships with tropospheric climate patterns,” *J. Clim.* **12** (9), 2719–2733 (1999).
12. E. S. Nesterov, *The North Atlantic Oscillation: The Atmosphere and the Ocean* (Triada, Moscow, 2013) [in Russian].
13. G. W. K. Moore and I. Renfrew, “Cold European winters: Interplay between the NAO and the East Atlantic mode,” *Atmos. Sci. Lett.* **13** (1), 1–8 (2012). <https://doi.org/10.1002/asl.356>
14. J. C. H. Chiang and D. J. Vimont, “Analogous Pacific and Atlantic meridional modes of tropical atmosphere–ocean variability,” *J. Clim.* **17** (21), 4143–4158 (2004). <https://doi.org/10.1175/JCLI4953.1>
15. P. Nobre and J. Shukla, “Variations of sea surface temperature, wind stress, and rainfall over the tropical Atlantic and South America,” *J. Clim.* **9** (10), 2464–2479 (1996).
16. B. Rajagopalan, Y. Kushnir, and Y. M. Tourre, “Observed decadal midlatitude and tropical Atlantic climate variability,” *Geophys. Res. Lett.* **25** (21), 3967–3970 (1998). <https://doi.org/10.1029/1998GL900065>
17. D. J. Vimont and J. P. Kossin, “The Atlantic Meridional Mode and hurricane activity,” *Geophys. Res. Lett.* **34** (7), L07709 (2007). <https://doi.org/10.1029/2007GL029683>
18. P. A. Vainovskii and V. N. Malinin, *Processing and Analysis Methods for Oceanological Information. Part 2. Multidimensional Analysis* (RGGMI, St. Petersburg, 1992) [in Russian].
19. B. C. Weare and R. E. Newell, “Empirical orthogonal analysis of Atlantic Ocean surface temperatures,” *Q. J. R. Meteorol. Soc.* **103** (437), 467–478 (1977). <https://doi.org/10.1002/qj.49710343707>
20. Y. M. Tourre, B. Rajagopalan, and Y. Kushnir, “Dominant patterns of climate variability in the Atlantic Ocean during the last 136 years,” *J. Clim.* **12** (8), 2285–2299 (1999).
21. A. I. Ugryumov “On large-scale oscillations of water surface temperature in the North Atlantic,” *Meteorol. Gidrol.* **5**, 12–22 (1973).
22. M. A. Balmaseda, A. Vidard, and D. L. T. Anderson, “The ECMWF Ocean Analysis System: ORA-S3,” *Mon. Weather. Rev.* **136** (8), 3018–3034 (2008). <https://doi.org/10.1175/2008MWR2433.1>
23. S. M. Uppala, P. W. Kållberg, A. J. Simmons, et al., “The ERA-40 re-analysis,” *Q. J. R. Meteorol. Soc.* **131B** (612), 2961–3012 (2005).
24. R. C. Pacanowski and S. G. H. Philander, “Parameterization of vertical mixing in numerical models of tropical oceans,” *J. Phys. Oceanogr.* **11** (11), 1443–1451 (1981).
25. N. E. Huang, Z. Shen, S. R. Long, et al., “The empirical mode decomposition and the Hilbert spectrum for non-linear and non-stationary time series analysis,” *Proc. R. Soc. London, Ser. A* **454** (1971), 903–995 (1998). <https://doi.org/10.1098/rspa.1998.0193>
26. *IPCC, 2013: Climate Change 2013: The Physical Science Basis. Contribution of Working Group I to the Fifth Assessment Report of the Intergovernmental Panel on Climate Change*, Ed. by T. F. Stocker, D. Qin, G.-K. Plattner, et al. (Cambridge University Press, Cambridge, UK and New York, NY, USA, 2013). <https://doi.org/10.1017/CBO9781107415324>
27. V. V. Zuev, V. A. Semenov, E. A. Shelekhova, S. K. Gullev, and P. Koltermann, “Evaluation of the impact of oceanic heat transport in the North Atlantic and Barents Sea on the Northern Hemispheric climate,” *Dokl. Earth Sci.* **445** (2), 1006–1010 (2012).
28. S. N. Moshonkin and N. A. Diansky, “Upper mixed layer temperature anomalies at the North Atlantic storm-track zone,” *Ann. Geophys.* **13**, 1015–1026 (1995).
29. J. A. Carton, S. A. Grodsky, and H. Liu, “Variability of the oceanic mixed layer, 1960–2004,” *J. Clim.* **21** (5), 1029–1047 (2008). <https://doi.org/10.1175/2007JCLI1798.1>
30. K. Lorbacher, D. Dommenges, P. P. Niiler, et al., “Ocean mixed layer depth: A subsurface proxy of ocean–atmosphere variability,” *J. Geophys. Res.* **111**, C07010 (2006). <https://doi.org/10.1029/2003JC002157>
31. C. Wang and L. Zhang, “Multidecadal ocean temperature and salinity variability in the tropical North Atlantic: Linking with the AMO, AMOC, and subtropical cell,” *J. Clim.* **6** (16), 6137–6162 (2013). <https://doi.org/10.1175/JCLI-D-12-00721.1>
32. N. A. Diansky and P. A. Sukhonos, “Multidecadal variability of hydro-thermodynamic characteristics and heat fluxes in North Atlantic,” in *Physical and Mathematical Modeling of Earth and Environment Processes. Springer Geology*. (Springer, Cham, 2018), pp. 125–137. https://doi.org/10.1007/978-3-319-77788-7_14
33. D. Kieke and I. Yashayaev, “Studies of Labrador Sea Water formation and variability in the subpolar North Atlantic in the light of international partnership and collaboration,” *Prog. Oceanogr.* **132**, 220–232 (2015). <https://doi.org/10.1016/j.pocan.2014.12.010>
34. N. J. Mantua, S. R. Hare, Y. Zhang, et al., “A Pacific interdecadal climate oscillation with impacts on salmon production,” *Bull. Amer. Meteorol. Soc.* **78** (6), 1069–1079 (1997).
35. G. V. Alekseev, N. I. Glok, A. V. Smirnov, and A. E. Vyazilova, “The influence of the North Atlantic on climate variations in the Barents Sea and their pre-

- dictability,” *Russ. Meteorol. Hydrol.* **41**, 544–558 (2016).
36. V. V. Ivanov and I. A. Repina, “The effect of seasonal variability of Atlantic water on the Arctic Sea ice cover,” *Izv., Atmos. Ocean. Phys.* **54** (1), 65–72 (2018).
37. D. R. Cayan, “Latent and sensible heat flux anomalies over the northern oceans: Driving the sea surface temperature,” *J. Phys. Oceanogr.* **22** (8), 859–881 (1992).
38. V. Slonosky and P. Yiou, “Does the NAO index represent zonal flow? The influence of the NAO on North Atlantic surface temperature,” *Clim. Dyn.* **19** (1), 17–30 (2002).
<https://doi.org/10.1007/s00382-001-0211-y>
39. E. Zorita, V. Kharin, and H. von Storch, “The atmospheric circulation and sea surface temperature in the North Atlantic area in winter: their interaction and relevance for Iberian precipitation,” *J. Clim.* **5** (10), 1097–1108 (1992).
40. R. J. Greatbatch, “The North Atlantic Oscillation,” *Stochast. Environ. Res. Risk Assessment* **14** (4–5), 213–242 (2000).
<https://doi.org/10.1007/s004770000047>
41. M. Latif, A. Grötzner, M. Münnich, et al., in *Decadal Climate Variability*, vol. 44 of *NATO ASI Series (Series I: Global Environmental Change)*, Ed. by D. L. T. Anderson and J. Willebrand (Springer, Berlin, Heidelberg, 1996).
https://doi.org/10.1007/978-3-662-03291-6_6
42. S. Peng and J. Fyfe, “The coupled patterns between sea level pressure and sea surface temperature in the midlatitude North Atlantic,” *J. Clim.* **9** (8), 1824–1839 (1996).
43. C. K. Folland, J. Knight, H. W. Linderholm, D. Fereday, S. Ineson, J. W. Hurrell, “The summer North Atlantic Oscillation: past, present, and future,” *J. Clim.* **22** (5), 1082–1103 (2009).
<https://doi.org/10.1175/2008JCLI2459.1>
44. P. Chang, L. Ji, and H. Li, “A decadal climate variation in the tropical Atlantic Ocean from thermodynamic air–sea interactions,” *Nature* **385** (6616), 516–518 (1997).
<https://doi.org/10.1038/385516a0>
45. S. P. Xie, “A dynamic ocean–atmosphere model of the tropical Atlantic decadal variability,” *J. Clim.* **12** (1), 64–70 (1999).
<https://doi.org/10.1175/1520-0442-12.1.64>

Translated by O. Ponomareva